Nuclear Engineering and Technology 58 (2026) 104077

Contents lists available at ScienceDirect

Nuclear Engineering and Technology

journal homepage: www.elsevier.com/locate/net

Original Article

# Enhanced fidelity of Monte Carlo coupled multi-physics simulations in the MCS code

Muhammad Imron [a,b,c], Deokjung Lee [a,d,*]

[a] Department of Nuclear Engineering, Ulsan National Institute of Science and Technology 50 UNIST-gil, Ulsan, 44919, Republic of Korea
[b] Department of Mechanical and Nuclear Engineering, Khalifa University of Science and Technology, Abu Dhabi, United Arab Emirates
[c] Emirates Nuclear Technology Center (ENTC), Khalifa University of Science and Technology, Abu Dhabi, United Arab Emirates
[d] Advanced Nuclear Technology and Services, 406-21 Jonga-ro, Jung-gu, Ulsan, 44429, Republic of Korea

ARTICLE INFO

*Keywords:*
Monte Carlo
Multi-physics
Functional expansion tally
High-fidelity
Thermal expansion

ABSTRACT

This study integrates previously developed methods to enhance the fidelity of direct whole-core Monte Carlo coupled multi-physics simulations in the MCS code. First, it introduces multi-physics simulations with spatially continuous material properties by using the Functional Expansion Tally combined with delta-tracking. Second, it incorporates on-the-fly thermal expansion of reactor core components during Monte Carlo particle tracking. To evaluate the accuracy and overall performance improvement of the framework, several numerical experiments were conducted at both the assembly and whole-core levels. The incorporation of spatially continuous material properties produces eigenvalue solutions that asymptotically converge to those from conventional cell-based discretized simulations with infinitesimally small cells as demonstrated in the assembly and whole-core problems. In the whole-core problem, the framework reduces simulation times by around threefold and requires 80 % less memory than the traditional cell-based discretization using very small cells, while maintaining the high-fidelity solutions. Whereas the numerical results for on-the-fly thermal expansion demonstrate that the observed trends in reactor reactivity due to thermal expansion align with previous studies. These findings suggest that integrating the multi-physics framework into reactor modeling can enhance simulation fidelity while reducing simulation time.

## 1. Introduction

Recent advancements in modern computing have enabled direct whole-core Monte Carlo (MC) coupled multi-physics simulations for large-scale reactor problems. In this approach, the multi-physics coupling between MC codes and thermal-hydraulic (TH) solvers is accomplished at the pin-by-pin level. Numerous examples of these reactor multi-physics simulations can be found in the literature [1–5], and they had demonstrated that such simulations are practically feasible for academic and research purposes. The results from such reactor multi-physics simulations have shown improved accuracy when compared to measured data and are often used as reference solutions for lower-order deterministic codes. However, according to Smith and Forget [6], there are still many important aspects of reactor simulations that must be incorporated to produce truly high-fidelity analysis tools.

While the work of Smith and Forget highlights many aspects to improve the fidelity of reactor calculations, this study attempts to solve two issues. First, inadequate spatial resolution, such as the improper modeling of radial temperature variations in fuel pellets, which is essential for accurately modeling spatial self-shielding effects [7]. Second, thermal expansion of the reactor core materials, which is often neglected in typical direct whole-core MC coupled multi-physics simulations.

There were attempts to solve the inadequate spatial resolution issue. One such method is Localized Delta Tracking (LTD) [7], which solves radial heat conduction within the fuel pellet using polynomial fitting. This approach allows for the determination of continuously varying radial fuel temperatures. By using LTD within the fuel pellet, MC multi-physics coupling can be achieved without requiring explicit radial discretization of the fuel pellet. However, LTD is limited to handling continuously varying fuel temperatures only in the radial direction. In the axial direction, traditional discretization of the problem domain is still necessary.

Leppänen [8] conducted another study using the Serpent 2 MC code

* Corresponding author. Department of Nuclear Engineering, Ulsan National Institute of Science and Technology 50 UNIST-gil, Ulsan, 44919, Republic of Korea.
*E-mail address:* deokjung@unist.ac.kr (D. Lee).

https://doi.org/10.1016/j.net.2025.104077
Received 6 February 2025; Received in revised form 10 November 2025; Accepted 9 December 2025
Available online 10 December 2025

to model continuous nonuniform density distributions. In this work, he implemented MC multi-physics coupling with a continuous moderator density, incorporating rejection sampling within a single material region. The study focused on continuous variations of coolant density and void fraction along the flow channel of a nuclear fuel assembly. However, it did not account for continuous variations in temperature or in the isotopic composition of materials dissolved in the moderator, such as boron. Later, Serpent 2 incorporated the modeling of continuous temperature variations. However, according to the Serpent manual [9], users are required to provide the expansion coefficients manually, and it remains unclear whether these coefficients are updated during multi-physics coupling. Moreover, the applicability of this feature to large reactor problems is still unknown.

One notable effort was made by Ellis [10], who employed the Functional Expansion Tally (FET) method [11,12] to achieve continuous representations of power. After multi-physics feedback calculations, the resulting continuous fuel pellet temperature and coolant density were also modeled using functional expansions. To facilitate MC particle tracking in a continuous medium, a modified version of Continuously Varying Material Tracking (CVMT) [13] was developed. These two methods were integrated to perform MC multi-physics simulations with continuously varying materials.

As for the thermal expansion implementation in direct multi-physics reactor calculations, thermal expansion is usually modeled in the MCS code by manually adjusting input files to uniformly expand the reactor core geometry and modify material densities. This method typically uses core-averaged nominal temperatures, as demonstrated by Palmtag et al. [14]. In Palmtag's work, thermal expansion was implemented by processing XML input files for the Consortium for Advanced Simulation of LWRs (CASL) core simulator code, VERA-CS [15], to uniformly adjust core dimensions and material densities. This process is accomplished by VERAIn ASCII input preprocessor. However, the VERAIn ASCII input preprocessor only allows thermal expansion at a pre-set and uniform temperature, which is typically set to the core-averaged temperature.

This work combines previous studies on MC coupled multi-physics reactor simulations with spatially continuous material properties [16] and on-the-fly thermal expansion [17], both of which were individually tested and evaluated, into a unified framework. Additionally, it evaluates the effectiveness of delta-tracking for MC coupled multi-physics reactor simulations with spatially continuous material properties in problems containing localized heavy neutron absorbers. Finally, this work also extends the scalability of previous studies to address whole-core problems.

## 2. Methodology

The proposed methodologies for MC coupled multi-physics reactor simulations with spatially continuous material properties and on-the-fly thermal expansion have been thoroughly detailed in our previous works [16,17]. In this study, we revisit the key concepts of these methodologies and provide insights into the subtle distinctions involved in their implementation for whole-core problems. Moreover, we discuss the challenges associated with integrating these two methodologies within the multi-physics framework.

### 2.1. Functional Expansion Tally

In conventional Monte Carlo (MC) multi-physics reactor simulations, the problem domain must be discretized into smaller cells, it is necessary to discretize the problem domain into smaller cells. The material properties, such as fuel temperature, moderator density, and the isotopic composition of materials diluted in the moderator, are assumed to be uniform within each cell. This discretization is essential for achieving adequate spatial resolution and accurately modeling variations in material properties. In particular, the radial discretization within the fuel pellets is essential for proper representation of the radial temperature profile of the pellets to correctly model the spatial self-shielding effects.

Although high spatial resolution can be achieved by discretizing the problem domain into smaller cells, this additional discretization can hinder MC particle tracking. Specifically, the cross-sections must be reconstructed each time a particle crosses a cell boundary. This also introduces higher memory burden, as data for numerous cells must be stored during the simulation. As a result, the added discretization in multi-physics simulations reduces the efficiency of the MC method in handling continuous geometry.

To address this spatial resolution issue, a multi-physics framework with spatially continuous material properties was proposed [16]. This methodology takes advantage of Functional Expansion Tally (FET) to obtain continuous representation of MC power tally. In the FET method, the actual power shape solution is approximated through a truncated linear combination of polynomials, with MC tallies used to calculate the coefficients of these polynomials. Therefore, the spatially continuous power distribution can be approximated using FET by expanding the tally quantity into a linear combination of polynomials $\psi\left(\vec{\xi}\right)$, as shown below:

$$f\left(\vec{\xi}\right) = \sum_{n=0}^{\infty} \bar{a}_n k_n \psi_n\left(\vec{\xi}\right), \tag{1}$$

$$\bar{a}_n = \langle f, \psi_n \rangle = \int_{\Gamma} f\left(\vec{\xi}\right) \psi_n\left(\vec{\xi}\right) \rho\left(\vec{\xi}\right) d\vec{\xi}\,. \tag{2}$$

Here, $\bar{a}_n$ represents the expansion coefficients, $\vec{\xi}$ denotes the neutron phase space comprising $\left(\vec{r}, \vec{\Omega}, E\right)$, and $k_n$ is the normalization constant, which can be determined based on the chosen polynomial basis set that can be expressed as:

$$k_n = \frac{1}{||\psi_n||^2}, \tag{3}$$

where

$$\left|\left|\psi_n\right|\right|^2 = \int_{\Gamma} \psi_n^2\left(\vec{\xi}\right) \rho\left(\vec{\xi}\right) d\vec{\xi}\,. \tag{4}$$

Lastly, the $\rho\left(\vec{\xi}\right)$ is the weighting function that shall be both complete and orthogonal with respect to $\psi_n\left(\vec{\xi}\right)$.

Fortunately, the integrals required to obtain the expansion coefficients in Eq. (2) can be easily calculated in MC simulations using both analog and collision-based estimators. The unbiased collision-based estimator for the coefficients $\bar{a}_n$, used to reconstruct the power (as per Eq. (1)), is defined as:

$$\bar{a}_n = \frac{1}{N} \sum_{i=1}^{N} \sum_{k=1}^{K_i} w_{i,k} \frac{\kappa\left(\vec{\xi}_{i,k}\right)}{\Sigma_t\left(\vec{\xi}_{i,k}\right)} \psi_n\left(\vec{\xi}_{i,k}\right) \rho\left(\vec{\xi}_{i,k}\right). \tag{5}$$

In Eq. (5), $N$ represents the total number of particles in each batch, $K_i$ is the total number of collisions for particle $i$, $w_{i,k}$ is the weight of particle $i$ at collision $k$, $\kappa\left(\vec{\xi}_{i,k}\right)$ is the energy released per fission at the phase space point $\vec{\xi}_{i,k}$, and $\Sigma_t\left(\vec{\xi}_{i,k}\right)$ is the total macroscopic cross section at the phase space point $\vec{\xi}_{i,k}$.

The use of FET in multi-physics simulations with spatially continuous material properties presents several challenges when combined with

thermal expansion. Thermal expansion causes the fuel pellet radius and length to change during particle transport. Since FET also needs this information, the FET geometry information must be modified accordingly. Furthermore, during FET tally reconstruction, these geometric changes in the fuel pellet must also be considered to ensure accurate tally reproduction.

### 2.2. Delta-tracking

Due to the continuous variation of material properties across the fuel pin, delta-tracking is used in place of conventional surface-tracking. Delta-tracking [18,19] is based on a rejection sampling scheme where the total interaction probability is made uniform by introducing majorant cross sections. As a result, a uniform distance to collision can be sampled by:

$$s = \frac{ln(\xi)}{\Sigma_{maj}(E)}. \tag{9}$$

Here, $\xi$ is a uniformly distributed random variable within the unit interval, and $\Sigma_{maj}(E)$ represents the majorant cross section. In this study, however, the total interaction probability is made uniform only within the delta-tracking region, which is typically defined at the assembly level.

To preserve the physical nature of neutron transport while allowing the neutron random walk to continue through multiple material regions, the interaction probability in each material is adjusted by introducing virtual collisions. Virtual collisions are rejected collisions that depend on the total cross section of the material where the neutron undergoes a collision. Practically, this involves performing rejection sampling where a collision is accepted as a physical collision with the following probability:

$$p = \frac{\Sigma_t(\vec{r}, E)}{\Sigma_{maj}(E)}. \tag{10}$$

If a collision is rejected as virtual, a new distance to collision is sampled, and the procedure is repeated from the beginning. While the value of the majorant cross section can be arbitrary, choosing it too large can result in poor efficiency of the rejection sampling routine. Therefore, it is common practice to select the majorant cross section such that:

$$\Sigma_{maj}(E) = \max[\Sigma_t(E)]. \tag{11}$$

The delta-tracking has a drawback in geometries with significant material heterogeneity, where the total cross sections of different materials vary considerably [20]. A common example is a Light Water Reactors' (LWRs) fuel assembly containing localized heavy absorbers, such as control rods or burnable absorber pins. In these cases, the absorber's cross section dominates the majorant cross section at low energy, even though it occupies only a small portion of the total volume. This leads to a low probability of rejection sampling shown in Eq. (10).

In the delta-tracking implementation within MCS, each fuel assembly has a distinct delta-tracking region, with each assembly having its own corresponding majorant cross-section. Therefore, when a particle crosses an assembly surface, the particle track must be terminated. Subsequently, a new sampling of the distance to collision must be calculated using a different majorant cross-section.

The implementation of delta-tracking for whole-core problems presents a challenge. Uninserted control rods within a fuel assembly can significantly reduce the efficiency of rejection sampling in that assembly. To address this issue, uninserted control rods outside the active region must be excluded from the delta-tracking region, where conventional surface tracking is used instead.

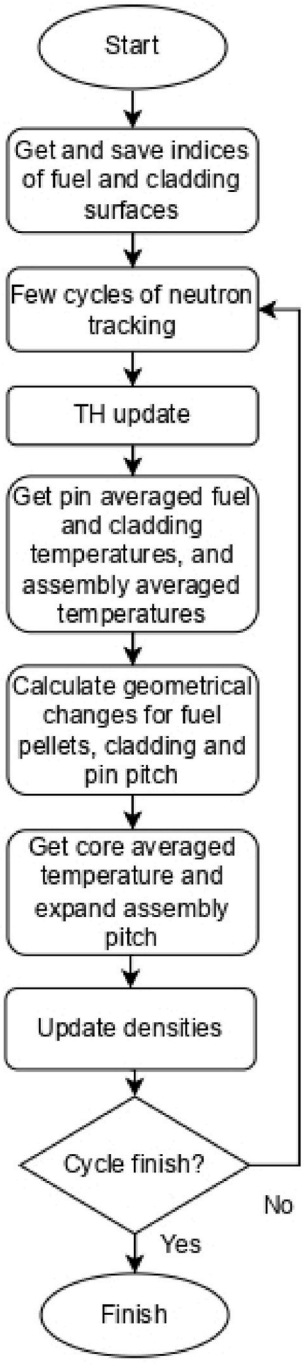


**Fig. 1.** Calculation of geometrical changes due to thermal expansion. Adapted from Ref. [15].

### 2.3. Thermal expansion

Many MC codes, including MCS, use Constructive Solid Geometry (CSG) to describe reactor geometry. Applying non-uniform geometrical expansion based on local temperatures in CSG can be difficult. This is because a single surface can be reused to define multiple cells in a universe, and a universe can also be reused to create a lattice. As a result, changes to one surface, such as those caused by thermal expansion, will affect all cells, universes, and lattices that use the same surface. One way to avoid this issue is by making separate copies of surfaces and cells, so each cell can be expanded according to its local temperature. However, this method becomes impractical for large reactor problems, as it

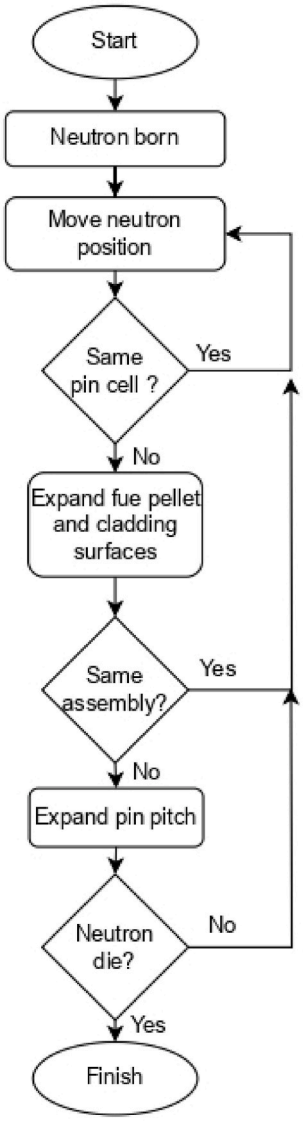


**Fig. 2.** On-the-fly thermal expansion during neutron tracking. Adapted from Ref. [15].

requires more memory and increases complexity.

To overcome this challenge, on-the-fly thermal expansion was introduced [17]. In this approach, when a particle enters a specific fuel pin, the geometry of the fuel pellet and cladding in that pin is expanded based on the corresponding local temperatures. These local temperatures can be either pin-averaged or assembly-averaged temperatures. In MCS, the fuel pellet expands in both radial and axial directions, while the cladding expands only radially, with its inner and outer radii assumed to expand equally. It is important to note that deformation is considered uniform both radially and axially, meaning phenomena like fuel cladding ballooning are not accounted for.

Once the geometrical changes due to thermal expansion are calculated during the thermal-hydraulic update as shown in Fig. 1, this information is used to thermally expand the core geometry on-the-fly during subsequent cycles of neutron tracking. When a neutron is located in a pin cell after performing a random walk, MCS checks whether it originated from another pin cell or from the same one. If it originated from another pin cell, the fuel pellet and cladding surfaces in that pin cell are expanded based on the previously calculated geometrical changes. Additionally, if the neutron came from another assembly, the pin pitches within that assembly are uniformly expanded as well. These steps are summarized in Fig. 2.

**Table 1**
Thermal expansion coefficients used in this study.

| Material | Thermal expansion coefficient ($K^{-1}$) |
|---|---|
| Zirconium alloys (fuel cladding) | $7.00 \times 10^{-6}$ |
| SS304 (core plate) | $1.78 \times 10^{-5}$ |
| Fuel pellet | $1.10 \times 10^{-5}$ |

### 2.4. Thermal expansion coefficients

The linear thermal expansion of solid materials with an isotropic crystal structure can be modeled using the formula:

$$L = L_0\left[1 + \alpha_L\left(T - T_{ref}\right)\right], \tag{12}$$

where $L$ represents the final length at temperature $T$, $L_0$ is the initial length at the reference temperature $T_{ref}$, and $\alpha_L$ is the linear thermal expansion coefficient. For area expansion, such as the area of a fuel pellet, the equation is:

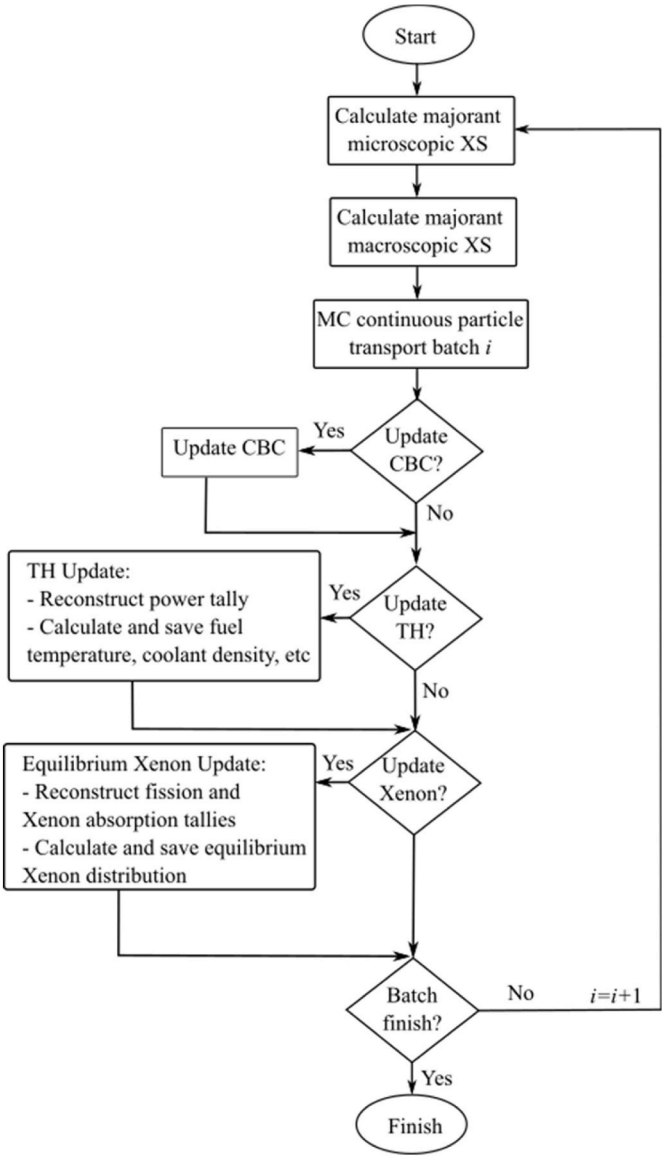


**Fig. 3.** Multi-physics coupling of the framework. Adapted from Ref. [14].

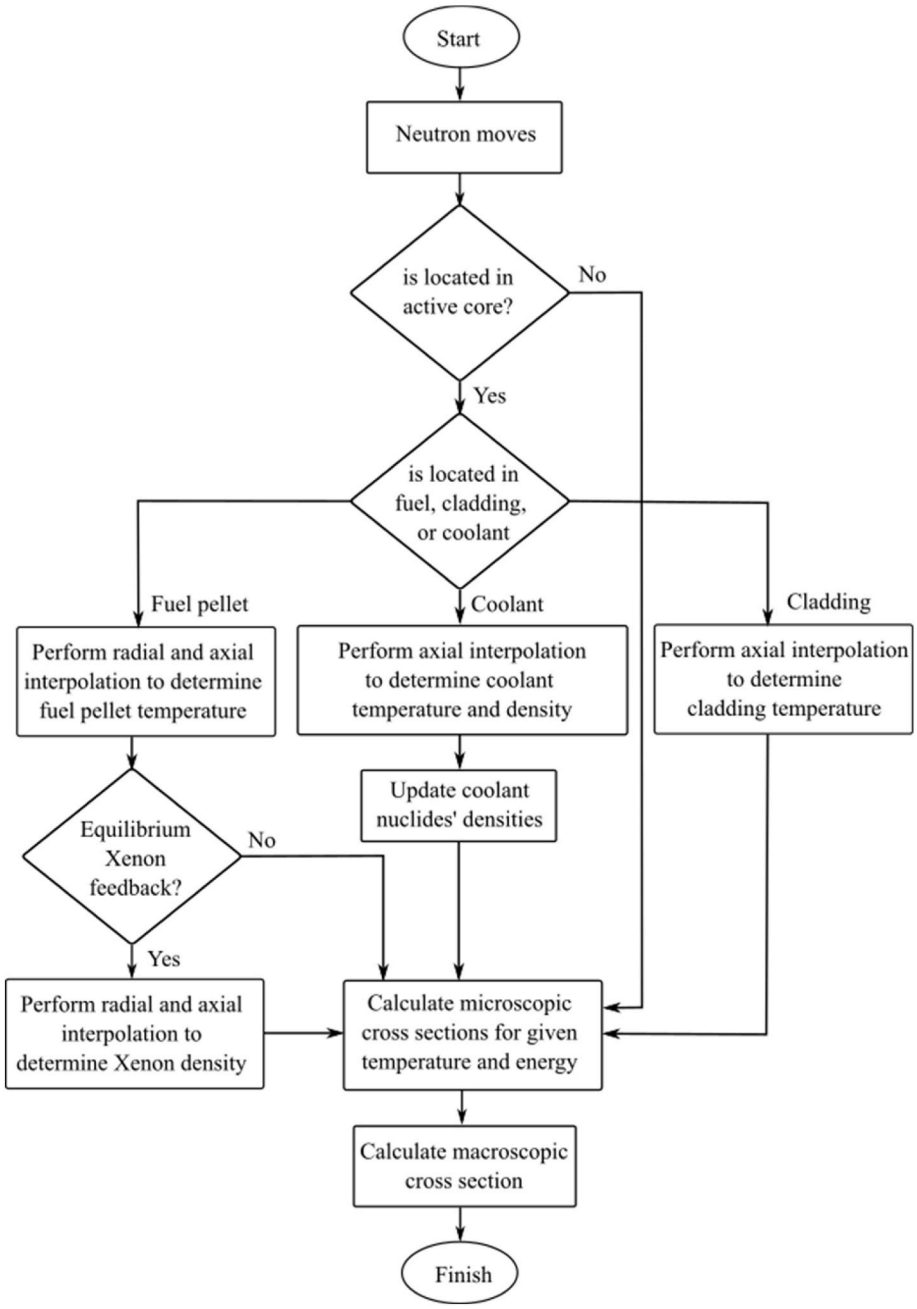


**Fig. 4.** Calculation flows to calculate macroscopic cross section in spatially continuous particle transport. Adapted from Ref. [14].

$$A = A_0\left[1 + \alpha_L\left(T - T_{ref}\right)\right]^2. \tag{13}$$

When materials expand, their mass remains the same, so the density must be adjusted to match the new dimensions. The adjusted density is calculated as:

$$\rho = \rho_0 \frac{V_0}{V}, \tag{14}$$

where $\rho$ and $V$ are th expanded density and volume, while $\rho_0$ and $V_0$ are the initial density and volume. The expanded volume is determined based on the expanded length $L$ and area $A$ from Eqs. (12) and (13).

Thermal expansion coefficients are crucial to accurately modeling how reactor materials expand. Detailed explanations of the methods used to determine these coefficients for typical LWR materials are provided in Ref. [14]. However, this study uses the coefficients provided by the STREAM code [21], which are summarized in Table 1.

It is worth mentioning that these coefficients are very similar to those reported by Palmtag et al. [14]. Additionally, this study focuses on modeling thermal expansion for the fuel pellet, cladding, pin pitch, and assembly pitch. The dimensions of absorber materials, such as control rods and burnable absorbers, are assumed to remain unchanged.

### 2.5. Multi-physics coupling

The multi-physics coupling is achieved by internally linking the TH solver with MCS. This integration enables automatic data exchange between MCS and the TH solver. Although the solvers must be compiled separately, they are connected via a static library. Linear power data from MCS is transferred to the TH solver, while TH parameters are updated by the TH solver and returned to MCS. These data transfer occur at the pin-by-pin level.

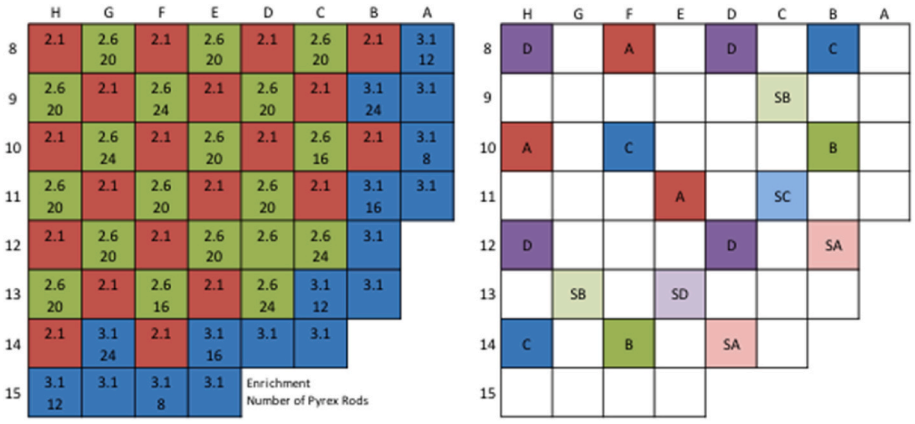


**Fig. 5.** VERA benchmark core configuration and control rods layout. Adapted from [22].

Particle delta-tracking in continuous media is carried out over several cycles, during which FET coefficients are tallied. After multiple cycles of particle transport, the TH conditions—as well as critical boron concentration (CBC) and Xenon distribution—are updated. During the TH update, the two-dimensional power distribution is reconstructed using the tallied FET coefficients. This reconstructed distribution is then used by the TH solver to calculate fuel, cladding, and coolant temperatures, along with coolant density. The resulting two-dimensional fuel temperature grids, along with one-dimensional cladding and coolant temperature grids and coolant density, are stored for each fuel pin. These TH condition grids serve as interpolation points for subsequent particle transport batches. This process is illustrated in Fig. 3.

The calculation of macroscopic cross sections for continuous particle tracking differs from the conventional method, where each cell assumes uniform material properties. In this framework, material properties are determined through interpolation, as illustrated in Fig. 4.

- When a neutron is in the fuel pellet, a two-dimensional interpolation in the axial and radial directions is used to determine the fuel temperature.
- If the neutron is in the coolant, a one-dimensional interpolation in the axial direction determines the temperature and density, which are then used to update the nuclide densities.
- For neutrons in the cladding, a one-dimensional axial interpolation provides the cladding temperature.

Once the interpolated temperatures and densities are established, microscopic cross sections are calculated for each nuclide based on the neutron energy and temperature. These are then used to compute the macroscopic cross section at the neutron's location.

Integrating FET with on-the-fly thermal expansion presents a challenge: as the fuel pellet undergoes thermal expansion, its radius and length change during particle transport. Since FET also requires this geometric information, these changes must be updated consistently. Furthermore, during FET tally reconstruction, the modified pellet geometry must be properly accounted for to ensure accurate tally reproduction.

This is accomplished by saving the geometrical changes caused by thermal expansion for each fuel pin at every thermal-hydraulic update (see Fig. 1). In subsequent particle-tracking cycles, this information is used to update the FET object data, including the fuel pellet radius and length. The corresponding normalized radius and length are also adjusted. In other words, the FET object data is dynamically updated according to the specific fuel pellet in which the particle is located. A similar procedure is applied before power reconstruction from tallied FET coefficients for each fuel pin, where the pellet geometry is again updated to reflect the latest thermal expansion data. This ensures that tallies and reconstructed power remain physically consistent with the deformed geometry.

## 3. Results and discussion

The applicability of the framework to enhance the fidelity of direct MC multi-physics simulations in the MCS code will be tested to several reactor problems. Additionally, the effectiveness of the methodology for problems containing high neutron absorbers will also be assessed. The test cases include both assembly and core problems, with geometries and material compositions adopted from the Virtual Environment for Reactor Applications (VERA) core physics benchmark [22].

For multi-physics feedback in this study, the radial heat conduction calculations within the fuel pellet were conducted using 10 radial rings, while a single mesh was employed for the gap and cladding regions. The resulting radial fuel temperature distribution was then averaged based on the number of radial cells used in the neutronic calculations.

In the conventional or cell-based approach, the problem geometry was discretized into several cells, with material properties such as temperature and density being uniform within each cell. This discretization was necessary to capture material property variations across the problem geometry. In contrast, in continuous material properties cases, explicit problem geometry discretization was unnecessary. Instead, the power and Xenon absorption rates distributions were reconstructed using 100 axial and 10 radial equidistant meshes for each pin during each TH update and equilibrium Xenon feedback, respectively. For tally reconstruction, seventh-order Legendre polynomials and ninth-order Zernike polynomials were used.

### 3.1. Benchmark descriptions

The reactor operational data for the VERA benchmark were taken from Watts Bar Generating Station Unit 1. This reactor is a 3411 MWth Westinghouse pressurized water reactor (PWR) with 193 fuel assemblies and an active core height of 365.76 cm. Each fuel assembly contains a 17x17 array of pins, consisting of 264 fuel pins, 24 guide tubes, and 1 instrumentation tube. Eight spacer grids are used for each assembly to maintain its structural integrity. Radially, the fuel-assembly pitch is 21.5 cm, with fuel pins within an assembly having pitch of 1.26 cm. The core configuration has a 0.04 cm inter-assembly gap which is essential to accommodate fuel assembly deformation due to thermal expansion.

During the first cycle, the reactor employed three different fuel enrichments: 2.11 %, 2.62 %, and 3.10 % by weight of U-235, and Pyrex burnable absorbers were used. Reactor regulation is provided by 57 reactor cluster rod assemblies (RCCAs), grouped into 8 banks, as illustrated in Fig. 5. Pyrex is a discrete burnable neutron absorber inserted into assembly guide tubes. These inserts can be placed in any assembly not located in a control rod position. The control rod is an axial stack of Silver-Indium-Cadmium (AIC) and boron carbide. A set of 24 control

**Table 2**
Infinite multiplication factors for assembly problems with and without thermal expansion modeling.

| Cases | # fuel pellet axial/radial discretization | $k_{inf}$ | |
|---|---|---|---|
| | | No TE | TE |
| A1 | 25/1 | 1.16400 (4) | 1.16321 (4) |
| A2 | 50/2 | 1.16443 (4) | 1.16350 (4) |
| A3 | 100/5 | 1.16449 (5) | 1.16368 (5) |
| FET | N/A | 1.16465 (4) | 1.16378 (4) |

rods are clustered into an RCCA to control and ensure a safe core shut down. The tips of the control rods are made from AIC and the remaining portions up to the plenum are made from boron carbide.

### 3.2. Three-dimensional assembly problem

In this subsection, the solutions to the three-dimensional assembly multi-physics problem using combined spatially continuous material properties and on-the-fly thermal expansion will be presented and discussed. This three-dimensional assembly multi-physics problem is identical to Problem #6 from the VERA benchmark, using 3.1 wt% enriched fuel pellets. The simulation is performed at hot full power (HFP), corresponding to 17.67 MW of thermal power, with 1300 ppm of boric acid dissolved in the coolant, and with no boron absorbers inserted into the guide tubes.

To compare the effect of thermal expansion, the simulations were performed both with and without thermal expansion being modeled. Additionally, four cases have been developed in this problem for comparison with the proposed framework. The first three cases, A1, A2, and A3, are traditional cell-based models where the problem domain is discretized into multiple cells. In case A1, the problem is divided into 25 equidistant axial cells without radial discretization. Case A2 refines this by using 50 equidistant axial cells and 2 equivolume radial rings in the fuel pellet to capture the temperature distribution within the pellet both radially and axially. Case A3 further increases the refinement to 100 equidistant axial cells and 5 equivolume radial rings. While FET case employs spatially continuous material properties. Each case simulated $3 \times 10^4$ particle histories per cycle, with a total of 12,500 cycles, of which 2500 were designated as active cycles.

Table 2 presents the solutions for all cases, both with and without thermal expansion. As can be seen, for both cases, the eigenvalues are generally increased as the fuel pellet discretization refines. That is due to better modeling of radial temperature profile of the fuel pellet when the radial discretization is refined which causes lower temperature in the fuel pellet periphery. Consequently, the absorption rate on the fuel pellet periphery is lower that leads to higher eigenvalue [16]. In other words, the spatial self-shielding phenomena is better modeled when there is finer radial discretization.

It can also be seen that the eigenvalues from the cell-based cases asymptotically converge to those from the FET cases as the cell sizes become infinitesimal. This demonstrates that higher accuracy is achievable with the multi-physics modeling using continuous material properties. This finding also confirms the correct implementation of the framework into the MCS code.

Moreover, due to the high concentration of boron dissolved in the coolant, thermal expansion modeling reduces the $k_{inf}$, thereby counteracting the effects of spatially continuous material modeling. This occurs because the moderator volume, which contains high boron, expands due to an increase in pin pitch. Consequently, the neutron absorption rate increases, leading to a lower eigenvalue. The impact of thermal expansion on the eigenvalue for a given boron concentration is consistent with the observations reported in Ref. [14].

### 3.3. Three-dimensional assembly problem with neutron absorbers

As mentioned earlier, the presence of localized heavy neutron absorbers reduces the rejection sampling efficiency in delta-tracking, thereby deteriorating the overall efficiency of MC particle tracking. This test problem aims to evaluate the extent of performance reduction caused by localized heavy neutron absorbers in typical LWR fuel assemblies.

The problem includes three types of fuel assemblies: one with Pyrex rods inserted into all 24 guide tubes, one with control rods inserted, and one without any neutron absorbers. While the Pyrex burnable poisons occupy almost the entire active core axially, the control rods are only inserted to a depth of 186 steps representing the rod position at the beginning of cycle. Note that all results do not model the thermal expansion.

The eigenvalue and running time comparisons relative to the FET cases are shown in Table 3. The fuel assembly without heavy neutron absorbers has the highest running time speedup relative to the spatially continuous cases. The FET case running time is more than 5 times faster compared to the A3 case with 5 radial discretization while resulting in better accuracy. This is primarily due to efficient rejection sampling for problems without localized neutron absorbers. The presence of Pyrex rods inserted into the guide tubes provides negligible effect on the running time speedup because the Pyrex rods location is not very localized since they occupy almost the entire active core axially.

In contrast, the presence of control rods is very localized, located in a small portion at the top of the active core. This leads to poor rejection sampling efficiency when delta-tracking is performed. The FET speedup compared to a 100/5 axial/radial discretization with control rods inserted at 186 steps is 2.6 times. This speedup is much smaller than for problems without the control rods inserted, which is around 5.1 times. The $k_{inf}$ solutions generally follow the same trend as in previous problems, where they converge to the FET case solutions for infinitesimal cells.

3.4. Whole-Core Problem.

The final test problem in this study is a whole-core problem with thermal expansion, based on Problem #7 of the VERA benchmark: a three-dimensional, beginning-of-cycle (BOC) physical reactor. This benchmark provides detailed descriptions of the reactor core geometry and internal structures. The bank D RCCA position for this problem is set to 215 steps, while other RCCAs are fully withdrawn. This test problem estimates the critical boron concentration at HFP.

**Table 3**
Infinite multiplication factors and relative running times for assembly problems with and without heavy neutron absorbers.

| Cases | # fuel pellet axial/radial discretization | No absorber | | Pyrex Absorber | | Control Rods 186 steps | |
|---|---|---|---|---|---|---|---|
| | | $k_{inf}$ | Relative running time | $k_{inf}$ | Relative running time | $k_{inf}$ | Relative running time |
| A1 | 25/1 | 1.16400 (4) | 1.6 | 0.95876 (4) | 1.5 | 1.15972 (4) | 0.8 |
| A2 | 50/2 | 1.16443 (4) | 2.3 | 0.95909 (4) | 2.1 | 1.16007 (4) | 1.1 |
| A3 | 100/5 | 1.16449 (5) | 5.1 | 0.95918 (4) | 4.7 | 1.16027 (4) | 2.6 |
| FET | N/A | 1.16465 (4) | 1.0[a] | 0.95929 (4) | 1.0[b] | 1.16047 (4) | 1.0[c] |

[a] The absolute wall-clock time for the FET case is 1.8 h with 70 MPI processes.
[b] The absolute wall-clock time for the FET case is 1.9 h with 70 MPI processes.
[c] The absolute wall-clock time for the FET case is 3.5 h with 70 MPI processes.

**Table 4**
Critical boron concentration search results for the whole-core problem.

| Cases | # fuel pellet axial/radial discretization | CBC (ppm) | |
|---|---|---|---|
| | | No TE | TE |
| A1 | 25/1 | 859.6 (0.2) | 855.7 (0.2) |
| A2 | 50/2 | 863.0 (0.2) | 859.3 (0.2) |
| A3 | 60/5 | 864.0 (0.2) | 859.9 (0.2) |
| FET | N/A | 866.2 (0.2) | 861.2 (0.2) |

As with the previous test problems, several cases were developed to compare the spatially continuous material approach with the cell-based approach. These cases, along with descriptions of cell discretization, are listed in Table 4. Note that all simulations utilized $6\times 10^4$ particles per cycle, over a total of 37,500 cycles, with 30,000 cycles designated as active. This number of particles histories produces axially averaged pin-power densities with maximum standard deviation around 0.6 %. This whole-core reactor problem is modeled in a quarter core.

Table 4 presents the CBC solutions for all cases. As expected, the CBC from cell-based cases converges to that from the FET case as the size of the cells decreases. As in the previous assembly problem, the effect of thermal expansion in this problem counteracts the modeling with spatially continuous material properties. That is because, with around 800 ppm boron concentration, thermal expansion still reduces reactivity.

Fig. 6 shows the assembly power map and its comparison between the spatially continuous case and cell-based case with 60/5 discretization. As observed, the maximum and minimum assembly power relative differences are approximately 0.3 %, with a root mean squared error (RMS) of 0.2 %. And the relative difference on axial power, shown in Fig. 7, is also less than 1.0 %. At the pin level, the normalized radial pin-power densities also exhibit good agreement between the spatially continuous case and cell-based case with 60/5 discretization, with an RMS of 0.3 %, and maximum and minimum relative differences of less than 2.0 %, as shown in Fig. 8. These results confirm that the solutions with spatially continuous material properties are well aligned with the cell-based cases that use very small cells.

To more clearly observe the effects of thermal expansion, another whole-core problem is run with boron concentration is set to zero. However, instead of estimating the critical boron concentration, this problem calculates the reactor eigenvalue. All other modeling parameters and cases are the same. Table 5 compiles all effective multiplication factors from all cases both with and without thermal expansion. For reactor problems with zero boron concentration, the thermal expansion modeling adds the reactivity by around 120 pcm as can be observed in Table 5. Also, as in the previous problems, the eigenvalue from cell-based cases converges to that from the FET case as the cells' size smaller.

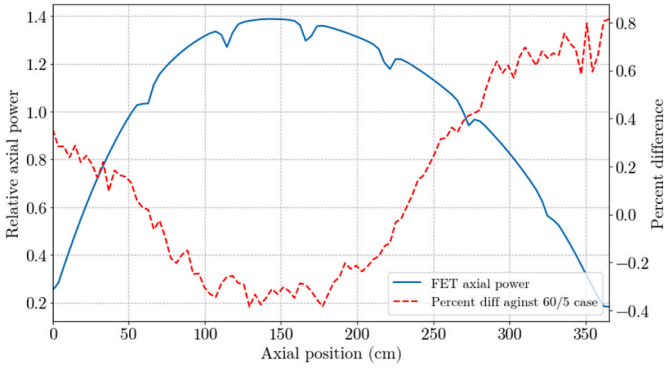


**Fig. 7.** Normalized axial power comparison for the whole-core problem between spatially continuous case and cell-based case with 60/5 discretization.

| | | | | | | | |
|---|---|---|---|---|---|---|---|
| 0.757 | 0.858 | 0.765 | 0.632 | | | | |
| 0.757 | 0.858 | 0.766 | 0.632 | | | | |
| 0.0% | 0.0% | -0.1% | 0.0% | | | | |
| 1.055 | 1.017 | 1.061 | 0.991 | 0.893 | 0.606 | | |
| 1.054 | 1.017 | 1.062 | 0.992 | 0.895 | 0.607 | | |
| 0.1% | 0.0% | -0.2% | -0.2% | -0.3% | -0.2% | | |
| 1.055 | 1.159 | 1.124 | 1.124 | 0.867 | 0.868 | 0.606 | |
| 1.054 | 1.159 | 1.125 | 1.125 | 0.869 | 0.870 | 0.607 | |
| 0.1% | 0.1% | -0.1% | -0.1% | -0.2% | -0.2% | -0.2% | |
| 1.157 | 1.079 | 1.186 | 1.079 | 1.245 | 0.867 | 0.893 | |
| 1.155 | 1.077 | 1.186 | 1.080 | 1.245 | 0.869 | 0.895 | |
| 0.2% | 0.1% | 0.0% | -0.1% | -0.1% | -0.2% | -0.3% | |
| 1.052 | 1.145 | 1.071 | 1.179 | 1.079 | 1.123 | 0.992 | 0.633 |
| 1.050 | 1.142 | 1.070 | 1.181 | 1.080 | 1.124 | 0.991 | 0.631 |
| 0.2% | 0.2% | 0.0% | -0.2% | -0.1% | -0.1% | 0.1% | 0.2% |
| 1.109 | 0.976 | 1.125 | 1.069 | 1.184 | 1.124 | 1.061 | 0.766 |
| 1.106 | 0.974 | 1.125 | 1.070 | 1.186 | 1.124 | 1.060 | 0.763 |
| 0.3% | 0.2% | 0.0% | -0.2% | -0.2% | 0.0% | 0.1% | 0.3% |
| 1.022 | 1.101 | 0.975 | 1.142 | 1.076 | 1.158 | 1.016 | 0.859 |
| 1.020 | 1.098 | 0.974 | 1.143 | 1.078 | 1.157 | 1.014 | 0.856 |
| 0.3% | 0.2% | 0.0% | -0.1% | -0.1% | 0.1% | 0.2% | 0.3% |
| 1.111 | 1.022 | 1.108 | 1.049 | 1.154 | 1.054 | 1.054 | 0.757 |
| 1.107 | 1.020 | 1.107 | 1.050 | 1.156 | 1.053 | 1.051 | 0.755 |
| 0.3% | 0.2% | 0.1% | 0.0% | -0.2% | 0.1% | 0.3% | 0.3% |

| FET CASE |
|---|
| 60/5 CASE |
| Rel. Diff. |

| | |
|---|---|
| Max. Diff | 0.3% |
| Min. Diff. | -0.3% |
| RMS | 0.2% |

**Fig. 6.** Assembly powers comparison for the whole-core problem between spatially continuous case and cell-based case with 60/5 discretization.

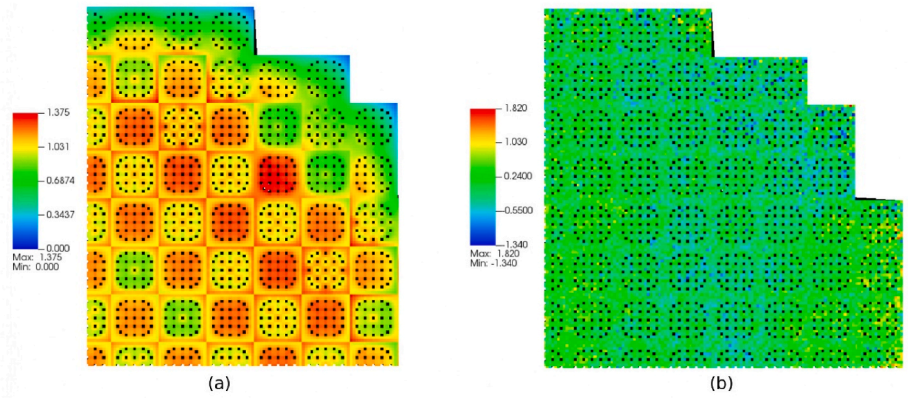


**Fig. 8.** Normalized radial pin-power densities of the FET case for the whole-core problems (a), and their comparisons against cell-based case with 60/5 discretization (b).

**Table 5**
Eigenvalue results for the whole-core problem with boron concentration set to 0 ppm.

| Cases | # fuel pellet axial/radial discretization | $k_{eff}$ | |
|---|---|---|---|
| | | No TE | TE |
| A1 | 25/1 | 1.09655 (2) | 1.09789 (2) |
| A2 | 50/2 | 1.09704 (2) | 1.09826 (2) |
| A3 | 60/5 | 1.09717 (2) | 1.09839 (2) |
| FET | N/A | 1.09743 (4) | 1.09860 (4) |

**Table 6**
Relative wall-clock time and memory usage for the whole-core problem without thermal expansion.

| Cases | # fuel pellet axial/radial discretization | Relative wall-clock time | Relative memory usage |
|---|---|---|---|
| A1 | 25/1 | 1.2 | 1.1 |
| A2 | 50/2 | 1.8 | 2.4 |
| A3 | 60/5 | 2.9 | 4.9 |
| FET | N/A | 1.0[a] | 1.0[b] |

[a] The absolute wall-clock time for the FET case is 14.3 h with a total of 70 MPI processes.

[b] The absolute memory usage for the FET case is 146.4 GB per node, with each node running 35 MPI processes.

### 3.4. Overall performance improvement

To improve the overall performance, the fully withdrawn RCCAs are not included in the delta-tracking region when delta-tracking is employed in the whole-core calculations. As previously demonstrated, the presence of localized strong neutron absorbers can significantly reduce the efficiency of rejection sampling. Fortunately, during typical reactor operation, only a single RCCA bank is inserted.

Table 6 presents the relative wall-clock time and memory usage of the whole-core problem without thermal expansion shown in Table 4. The memory usage was measured in the Ubuntu operating system using the `free -m` command during the simulation. As can be seen in Table 6, the FET case only requires one-third of the simulation time to achieve similar or even better accuracy compared to the case with 60/5 axial/radial cell discretization.

Additionally, the FET case requires only 20 % of the RAM compared to the E3 case. This reduction in memory usage is mainly due to the fewer number of cells employed in the FET case. Although there is additional memory needed to store the FET coefficients, the number of coefficients is too small to offset the overall memory reduction. This demonstrates that the use of spatially continuous materials with FET not only achieves better accuracy with less simulation time but also requires lower memory usage.

## 4. Conclusions

The introduction of MC multi-physics framework with spatially continuous material properties using FET and delta-tracking combined with on-the-fly thermal expansion was introduced in this study. FET was employed to obtain continuous representations of power, which enables the calculation of nearly continuous material properties distributions such as temperature and density. Then using spatial interpolation, material properties at any spatial points can be calculated. Meanwhile, delta-tracking was utilized as a particle tracking method in a continuous medium.

On-the-fly thermal expansion was integrated to address the challenge that the core temperature profile required for TE is not known as a priori and is typically non-uniform across the core. By incorporating on-the-fly thermal expansion, the core geometry can be modified on-the-fly during particle tracking based on the local temperatures at the pin-level.

The framework presented in this study was tested on several reactor problems, both on assembly and core levels. The continuous representation of the intra-fuel pellet profile enabled by MC multi-physics coupling with spatially continuous material properties captures more precise resonance absorption at the fuel-pellet periphery. This leads to a more accurate eigenvalue solution from the framework. Moreover, in the whole-core reactor problem, this approach reproduces high-fidelity solutions for both eigenvalue and pin powers, while accelerating the simulation time to almost three times faster and requiring 80 % less memory than the cell-based discretization approach using very small cells.

The most natural extension of this framework is the integration of continuous material depletion. However, accurately modeling radial U-238 absorption rate profile remains challenging due to its steep radial gradient. Unfortunately, such radial profiles cannot be adequately represented using FET with Zernike polynomials, as FETs are only suited for approximating smooth functions. Using piecewise function, as in the axial direction, is also not a solution because Zernike function is valid for a unit disk, not an annulus. Therefore, alternative polynomial functions, or perhaps completely different approach is necessary to obtain a continuous radial profile for U-238 absorption rates.

In conclusion, this study demonstrated that the integration of MC multi-physics coupling with spatially continuous material properties and on-the-fly thermal expansion capabilities significantly enhances the accuracy and efficiency of reactor simulations.

## CRediT authorship contribution statement

**Muhammad Imron:** Writing – original draft, Visualization, Validation, Software, Methodology, Investigation, Data curation. **Deokjung Lee:** Writing – review & editing, Supervision, Resources, Project administration, Funding acquisition, Conceptualization.

## Declaration of generative AI in scientific writing

During the preparation of this work the authors used ChatGPT-4o to improve readability, clarity, and conciseness of the writing. After using this tool, the authors reviewed and edited the content as needed and take full responsibility for the content of the publication.

## Declaration of interests

The authors declare that they have no known competing financial interests or personal relationships that could have appeared to influence the work reported in this paper.

## Acknowledgments

This work was partially supported by the Innovative Small Modular Reactor Development Agency grant funded by the Korea Government (MSIT) (No. RS-2023-00258205). This work was also supported by the National Research Foundation of Korea (NRF) grant funded by the Korea government (MSIT) (No. NRF-2019M2D2A1A03058371).

## References

[1] M. Daeubler, A. Ivanov, B.L. Sjenitzer, V. Sanchez, R. Stieglitz, R. Macian-Juan, High-fidelity coupled monte carlo neutron transport and thermal-hydraulic simulations using serpent 2/SUBCHANFLOW, Ann. Nucl. Energy 83 (2015) 352–375, https://doi.org/10.1016/J.ANUCENE.2015.03.040.

[2] D.J. Kelly, A.E. Kelly, B.N. Aviles, A.T. Godfrey, R.K. Salko, B.S. Collins, MC21/CTF and VERA multiphysics solutions to VERA core physics benchmark progression problems 6 and 7, Nucl. Eng. Technol. 49 (2017) 1326–1338, https://doi.org/10.1016/j.net.2017.07.016.

[3] Y. Ma, S. Liu, Z. Luo, S. Huang, K. Li, K. Wang, G. Yu, H. Yu, RMC/CTF multiphysics solutions to VERA core physics benchmark problem 9, Ann. Nucl. Energy 133 (2019) 837–852, https://doi.org/10.1016/j.anucene.2019.07.033.

[4] T.D.C. Nguyen, H. Lee, S. Choi, D. Lee, MCS/TH1D analysis of VERA whole-core multi-cycle depletion problems, Ann. Nucl. Energy 139 (2020), https://doi.org/10.1016/j.anucene.2019.107271.

[5] J. Yu, H. Lee, H. Kim, Z. Peng, D. Lee, Coupled Neutronics–Thermal-hydraulic simulation of BEAVRS cycle 1 depletion by the MCS/CTF code system, Nucl. Technol. 206 (2020) 728–742, https://doi.org/10.1080/00295450.2019.1677107.

[6] B.F.K. Smith, Challenges in the development of high-fidelity LWR core neutronics tools, in: International Conference on Mathematics and Computational Methods Applied to Nuclear Science and Engineering, M&C 2013, Sun Valley, ID, 2013.

[7] N. Choi, H.G. Joo, Analytic treatment of intra-fuel-rod temperature distributions in the GPU-based continuous energy Monte Carlo code PRAGMA, in: Transactions of the American Nuclear Society Annual Meeting, 2020.

[8] J. Leppänen, Modeling of nonuniform density distributions in the serpent 2 monte Carlo Code, Nucl. Sci. Eng. 174 (2013) 318–325, https://doi.org/10.13182/NSE12-54.

[9] Serpent Development Team, Serpent 2 user Manual: functional expansion tally based interface (Type 31 and 32), (n.d.). https://serpent.vtt.fi/mediawiki/index.php/Multi-physics_interface#Functional_expansion_tally_based_interface_(type_31_and_32).

[10] M.S. Ellis, Methods for Including Multiphysics Feedback in Monte Carlo Reactor Physics Calculations, Massachusetts Institute of Technology, Thesis, 2017. https://dspace.mit.edu/handle/1721.1/112381.

[11] W.L. Chadsey, C.W. Wilson, V.W. Pine, W.L. Chadsey, C.W. Wilson, V.W. Pine, X-ray photoemission calculations, IEEE Trans. Nucl. Sci. 22 (1975) 2345–2350, https://doi.org/10.1109/TNS.1975.4328131.

[12] D. Griesheimer, Functional Expansion Tallies for Monte Carlo Simulations, University of Michigan, 2005.

[13] F.B. Brown, W.R. Martin, Direct sampling of monte carlo flight paths in media with continuously varying cross-sections, in: Proc. ANS Mathematics & Computation Topical Meeting, 2003.

[14] S. Palmtag, B. Kochunas, D. Jabaay, Z. Han, T. Downar, Modeling thermal expansion in VERA-CS, in: Proceeding of International Conference on Mathematics & Computational Methods (M&C 2017), Jeju, South Korea, 2017.

[15] M. Sieger, R.K. Salko Jr., B. Kochunas, B. Adams, R. Williamson, VERA 3.3 Release Notes, CASL Technical Report: CASL-U-2015-0042-000, 2015.

[16] M. Imron, D. Lee, Monte carlo coupled multi-Physics with spatially continuous material properties, Ann. Nucl. Energy 210 (2025) 110856, https://doi.org/10.1016/j.anucene.2024.110856.

[17] M. Imron, D. Lee, On-the-fly thermal expansion for Monte carlo multi-physics reactor simulations, Frontiers in Nuclear Engineering 3 (2024) 1483520.

[18] E. Woodcock, T. Murphy, P. Hemmings, S. Longworth, Techniques used in the GEM code for Monte carlo neutronics calculations in reactors and other systems of complex geometry, in: Proc. Conf. Applications of Computing Methods to Reactor Problems, Argonne National Laboratory, 1965.

[19] J. Leppänen, On the use of delta-tracking and the collision flux estimator in the serpent 2 Monte Carlo particle transport code, Ann. Nucl. Energy 105 (2017) 161–167, https://doi.org/10.1016/j.anucene.2017.03.006.

[20] J. Leppänen, Performance of Woodcock delta-tracking in lattice physics applications using the Serpent Monte Carlo reactor physics burnup calculation code, Ann. Nucl. Energy 37 (2010) 715–722, https://doi.org/10.1016/j.anucene.2010.01.011.

[21] S. Choi, W. Kim, J. Choe, W. Lee, H. Kim, B. Ebiwonjumi, E. Jeong, K. Kim, D. Yun, H. Lee, D. Lee, Development of high-fidelity neutron transport code STREAM, Comput. Phys. Commun. 264 (2021) 107915, https://doi.org/10.1016/j.cpc.2021.107915.

[22] A.T. Godfrey, VERA Core Physics Benchmark Progression Problem Specifications, U.S. Department of Energy, 2014.